Title

Proteome-wide Profiling of Clinical PARP Inhibitors Reveals Compound-Specific Secondary Targets

Journal

Cell Chemical Biology, 23(12)

ISSN

2451-9456

Authors

Knezevic, Claire E
Wright, Gabriela
Rix, Lily L Remsing
et al.

Publication Date

2016-12-01

DOI

10.1016/j.chembiol.2016.10.011

Peer reviewed

HHS Public Access

Author manuscript

Cell Chem Biol. Author manuscript; available in PMC 2017 December 22.

Published in final edited form as:

Cell Chem Biol. 2016 December 22; 23(12): 1490–1503. doi:10.1016/j.chembiol.2016.10.011.

Proteome-wide profiling of clinical PARP inhibitors reveals compound-specific secondary targets

Claire E. Knezevic[#1,‡], **Gabriela Wright**[#1], **Lily L. Remsing Rix**[1], **Woosuk Kim**[2,3], **Brent M. Kuenzi**[1,4], **Yunting Luo**[5], **January M. Watters**[1,4], **John M. Koomen**[6], **Eric B. Haura**[7], **Alvaro N. Monteiro**[8], **Caius Radu**[2,3], **Harshani R. Lawrence**[1,5], and **Uwe Rix**[1,*]

[1]Department of Drug Discovery, H. Lee Moffitt Cancer Center & Research Institute, Tampa, FL, USA

[2]Department of Molecular and Medical Pharmacology, University of California, Los Angeles, Los Angeles, CA, USA

[3]Ahmanson Translational Imaging Division, University of California, Los Angeles, Los Angeles, CA, USA

[4]Cancer Biology Ph.D. Program, University of South Florida, Tampa, FL, USA

[5]Chemical Biology Core, H. Lee Moffitt Cancer Center & Research Institute, Tampa, FL, USA

[6]Department of Molecular Oncology, H. Lee Moffitt Cancer Center & Research Institute, Tampa, FL, USA

[7]Department of Thoracic Oncology, H. Lee Moffitt Cancer Center & Research Institute, Tampa, FL, USA

[8]Department of Cancer Epidemiology, H. Lee Moffitt Cancer Center & Research Institute, Tampa, FL, USA

[#] These authors contributed equally to this work.

Summary

PARP inhibitors (PARPi) are a promising class of targeted cancer drugs, but their individual target profiles beyond the PARP family, which could result in differential clinical utility or toxicity, are unknown. Using an unbiased, mass spectrometry-based chemical proteomics approach, we generated a comparative proteome-wide target map of the four clinical PARPi olaparib, veliparib,

[*]corresponding author: uwe.rix@moffitt.org.

[‡]current address: Department of Pathology, Johns Hopkins School of Medicine, Baltimore, MD, USA

Lead contact: Uwe Rix

Author contributions

Conceptualization, UR; Investigation, CEK, GW, WK, LLRR, YL, JMW, and UR; Formal Analysis, CEK, GW, and UR; Writing – Original Draft, CEK, GW, and UR; Writing – Review & Editing, CEK, GW, LLRR, BMK, ANM, JMK, EBH, and UR; Funding Acquisition, EBH and UR; Software, BMK; Visualization, BMK, ANM, CEK, GW, and UR; Resources, JMK, CR, HRL, and UR; Supervision, CR, HRL, JMK, and UR.

The remaining authors declare no competing financial interests.

niraparib, and rucaparib. PARPi as a class displayed high target selectivity. However, in addition to the canonical targets PARP1, PARP2 and several of their binding partners, we also identified hexose-6-phosphate dehydrogenase (H6PD) and deoxycytidine kinase (DCK) as previously unrecognized targets of rucaparib and niraparib, respectively. Subsequent functional validation suggested that inhibition of DCK by niraparib could have detrimental effects when combined with nucleoside analog pro-drugs. *H6PD* silencing can cause apoptosis and further sensitize cells to PARPi, suggesting that H6PD may be, in addition to its established role in metabolic disorders, a new anticancer target.

Graphical abstract

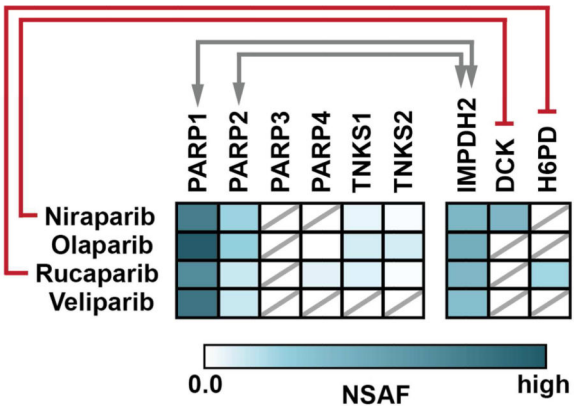

Introduction

Poly(ADP-ribose) polymerase-1 (PARP1) inhibition confers synthetic lethality to *BRCA1/2*-mutant cancer cells, which represents a developing paradigm for anticancer therapy (Bryant et al., 2005; Farmer et al., 2005; Kaelin, 2005). The clinical promise of PARP1 as an anticancer target is illustrated by the numerous PARP1 inhibitors (PARPi) currently in clinical trials in a wide range of cancer types, both as single agents and in combination with conventional chemotherapy (Lee et al., 2014; Scott et al., 2015). So far, five compounds have reached phase III studies and one of these, olaparib, is approved for the treatment of *BRCA1/2*-deficient ovarian cancers. However, small molecule drugs are often not exclusively specific for their intended targets, which has been well documented, for instance, with tyrosine kinase inhibitors (Bantscheff et al., 2007; Davis et al., 2011; Rix et al., 2007). Such off-target activity can be a liability as it can cause toxicity. Conversely, inhibition of multiple targets, including unintended/non-canonical targets, may also enhance overall efficacy (polypharmacology) or enable drug repurposing (Overington et al., 2006). Thus, understanding the molecular interaction landscape of PARPi will be relevant in many cancer types, including both wild-type and *BRCA1/2*-mutant settings.

All PARPi have similar potency for the *in vitro* inhibition of PARP1/2 enzymatic activity, but their cellular activity varies significantly (Chuang et al., 2012). This has mostly been attributed to their differential ability to trap PARP1 onto sites of DNA damage (Murai et al., 2012; Strom et al., 2011), although the exact mechanisms are not fully understood and its relevance across different cell types is not known (Hopkins et al., 2015; Scott et al., 2015).

Since all PARPi contain a benzamide pharmacophore designed to fit into the nicotinamide region of the NAD^+-binding pocket of PARP1 and there are many other NAD^+-binding proteins, Rouleau et al. and Tulin have proposed that PARPi may have broad and idiosyncratic off-target profiles (Rouleau et al., 2010; Tulin, 2011). Consistent with this hypothesis, a recent study demonstrated that the binding profiles of PARPi, including those of some clinical candidates, vary even within the PARP protein family (Wahlberg et al., 2012). The Wahlberg study investigated the ability of a library of PARPi to bind to the catalytic domains of PARP family proteins *in vitro*, and suggests that different PARPi may have distinct target patterns across this protein family.

Building upon these literature reports, we hypothesized that PARPi may also have differential target profiles outside of the PARP protein family and that this could be investigated using endogenously expressed proteins surveyed in an unbiased manner. Thus, we determined the proteome-wide protein target profiles of the four PARPi niraparib, olaparib, rucaparib, and veliparib, which are all currently in advanced clinical development, by chemical proteomics.

Results

PARPi analogs are robust PARP1/2 affinity probes

In order to generate an unbiased and global view of PARPi interacting proteins, we chose a mass spectrometry (MS)-based chemical proteomics approach. In this strategy, drug affinity matrices are prepared by the immobilization of PARPi analogs and the cellular proteins that bind to these matrices are identified using LC-MS/MS (Rix and Superti-Furga, 2009; Ziegler et al., 2013). Hypothesizing that non-canonical PARPi targets would likely be NAD^+-binding proteins, analogs were designed to retain key features needed for NAD^+-pocket binding. To guide this design, publically available co-crystal structures of PARPi with PARP family proteins were used. For instance, the co-crystal structure of tankyrase 2 and olaparib (pdb: 3U9Y) suggests that a tether attached at the cyclopropylamide distal to the benzamide pharmacophore would extend into the solvent space and not interfere with protein binding (Narwal et al., 2012). Modified versions of niraparib, olaparib, rucaparib, and veliparib with propylamine linkers suitable for coupling to solid supports were synthesized accordingly (Figures 1A and S1). As expected, these modifications had little-to-no effect on inhibition of PARP1 activity *in vitro* (PARPi vs c-PARPi, Figure 1B), confirming their suitability for use as affinity probes.

Each PARPi analog was individually immobilized on beads and incubated with CAL-51 total cell lysate. CAL-51 triple-negative breast cancer cells are *PTEN*-null and have activating *PIK3CA* mutations, which are associated with defects in DNA damage repair by homologous recombination and with synthetic lethality with PARPi (Mendes-Pereira et al., 2009). Accordingly, and in agreement with previous reports (Chuang et al., 2012), CAL-51 cells are sensitive to PARPi treatment (Figure 1C) and represent tumor types for which PARPi are investigated in the clinic. PARPi-sensitive cells were chosen to increase the likelihood of identifying targets that contribute to drug activity. Immunoblotting of the drug affinity eluates confirmed that, as expected, PARP1 and PARP2 were specifically enriched

by all PARPi matrices and depleted by competition with free PARPi, indicating binding specificity (Figure 1D).

PARPi matrices enrich for PARP1/2 protein complexes

Proteins enriched with the PARPi affinity matrices were eluted and subjected to in-gel trypsin digestion. Subsequent analysis of the resulting peptides by LC-MS/MS and database search using Mascot identified more than 1,200 proteins (Table S1). Relative quantification of triplicate analyses was achieved using normalized spectral abundance factors (NSAF), an established method for quantification of label-free proteomics data (Zybailov et al., 2007). Beyond PARP1/2, the NSAF-based analysis suggested only few and relatively weak interactions with other PARP family members in these cells, such as PARP4 and the tankyrases (Figure 2A and Table S2). PARP3 was not observed likely due to incompatibility of immobilization of PARPi with the unique structure of the NAD^+ binding pocket of this particular PARP family member (Lehtio et al., 2009). However, we identified a number of non-PARP family proteins as specific binders of the PARPi matrices (Table S3). Querying publically available protein-protein interaction (PPI) databases identified many known binding partners of PARP1 (and PARP2) within the resulting network, such as DNA ligase III (LIG3), XRCC1, Ku70 (XRCC6) and Ku80 (XRCC5), some of which may bind to PARP1/2 via PARylation (Figure 2B)(Gagne et al., 2012; Jungmichel et al., 2013).

In addition, we observed several NAD^+- and nucleotide-binding proteins that are not known to bind to PARP family proteins. Proteins such as these could therefore be new PARPi targets. One prominent NAD^+-binding protein, inosine monophosphate dehydrogenase 2 (IMPDH2), was identified with all four PARPi (Figures 2B and 2C). IMPDH2 converts inosine monophosphate to xanthosine monophosphate as part of the *de novo* guanine synthesis pathway. Although IMPDH2 binds to NAD^+, this protein co-immunoprecipitated with endogenous PARP1 and PARP2 (Figure 2D), indicating that IMPDH2 is more likely a new binding partner of PARP1/2 rather than a common drug target of all four PARPi. Consistent with this, c-rucaparib pulldown from PARP1-depleted stable shPARP1 CAL-51 cells, in comparison to parental CAL-51 cells, shows a similarly diminished enrichment of IMPDH2 as the known PARP1-binder Ku80 (Figure S2A). The small amount of IMPDH2 enriched from the shPARP1 lysate is likely due to the PARP2/IMPDH2 interaction. In contrast, the enrichment of the novel rucaparib target H6PD is not significantly diminished in the shPARP1 lysate.

Using an *in vitro* assay, no significant inhibition of IMPDH2 was observed with any of the four PARPi (IC_{50}'s ≥ 100 μM) (Figure S2B). However, we found that the presence of 20 μM PARPi abrogated the co-immunoprecipitation of IMPDH2 with PARP1 without affecting PARP1 recovery (Figure S2C). This suggests a complex interplay of drug-induced conformational changes of PARP1 and its binding to antibody and IMPDH2.

To further aid in the identification of compound-specific PARPi candidate targets, SAINTexpress statistical analysis was employed (Figure 3 and Table S4) (Teo et al., 2014). SAINT scores reflect the probability of a true interaction based on the SAINT algorithm and the provided controls. Comparison of each c-PARPi enrichment to its matched competition and ampicillin control experiments (Table S5) reveals, consistent with our network analysis,

that at a SAINT score cut-off of 0.9, PARPi enrich for PARP1/2 and their interacting proteins (Figures 3A-D). To identify any target candidates unique to individual PARPi, each c-PARPi enrichment was compared, using SAINTexpress, to the other three c-PARPi enrichments. Neither c-olaparib nor c-veliparib showed any unique interacting proteins with SAINT scores above a cut-off of 0.5 (Figures 3F and 3H), while both c-niraparib and c-rucaparib displayed several candidate target proteins (Figures 3E and 3G). Using both the network and SAINT analysis, we identified in total 18 targets/target candidates for rucaparib, 16 for niraparib, 10 for olaparib and 7 for veliparib, including already validated PARP family members. While we had expected predominantly NAD^+-binding proteins as target candidates, a number of interesting proteins that either do not utilize or do not exclusively utilize NAD^+ were observed. Target candidates were thus prioritized based on fold change and SAINT score, which together reflect uniqueness and therefore a higher likelihood for direct drug binding, number of peptides observed, which often correlates with interaction strength, and relevance to cancer.

Niraparib inhibits deoxycytidine kinase and reduces cytarabine activity

Cross-comparison of c-niraparib to c-veliparib, c-olaparib, and c-rucaparib-enriched samples highlighted some potentially novel targets that were specific for niraparib over all other PARPi tested, such as citron kinase (CIT), ferrochelatase (FECH) and deoxycytidine kinase (DCK) (Figure 3E). Whereas CIT was assigned a high SAINT score and displayed a high fold change, its large size of 230 kDa and the relatively few peptides identified for this protein (Table S1) suggest that CIT is likely not a strong niraparib interactor. The mitochondrial enzyme FECH was recently found to bind to many small molecule kinase inhibitors (Klaeger et al., 2016; Savitski et al., 2014) and was observed in our data with niraparib, but, similarly to CIT, showed only low spectral counts (Table S1). The most prominent unique niraparib candidate identified was DCK, which is responsible for the monophosphorylation of deoxycytidine, deoxyadenosine, and deoxyguanosine in the rate-limiting step of the nucleotide salvage pathway. Furthermore, DCK is essential for the phosphorylation and activation of antimetabolite prodrugs, such as gemcitabine and cytarabine (Figure 4A) (Galmarini et al., 2001).

Enrichment of DCK by c-niraparib was confirmed by immunoblotting, with partial competition by free niraparib (Figure 4B). Cross-competition with the natural substrate deoxycytidine or the potent DCK inhibitor DI-39 (Nathanson et al., 2014) resulted in complete loss of DCK binding to the c-niraparib matrix while having no effect on PARP1 recovery (Figure 4C). This strongly supports a direct interaction of c-niraparib with DCK. Docking of niraparib into the substrate- and inhibitor-binding pocket of DCK (pdb: 4KCG, Figure S3A) demonstrates the feasibility of this binding mode. Measurement of DCK activity in cell-free extracts confirmed specific inhibition of DCK by niraparib compared to the other PARPi (Figure S3B). It is well established that inhibition of DCK in cancer cells prevents conversion of nucleoside analogs to their cytotoxic triphosphates (Laing et al., 2009). To determine the cellular effects of niraparib on DCK-dependent nucleoside analog anticancer activity, we evaluated the potency of cytarabine in the absence and presence of PARPi in A549 lung cancer cells, which are relatively insensitive to PARP1 inhibition (Byers et al., 2012). Using the specific DCK inhibitor DI-39 as a positive control, niraparib

dose-dependently rescued A549 cells from cytarabine toxicity, albeit at micromolar concentrations, whereas the other three PARPi did not provide any rescue (Figure 4D). This suggests that niraparib can inhibit DCK in intact cancer cells.

Rucaparib inhibits hexose-6-phosphate dehydrogenase

Analysis of c-rucaparib affinity eluates in comparison with the other PARPi interaction data sets highlighted several potentially novel targets that were specific for rucaparib over all other PARPi tested. The kinases PIM1 and DYRK1A are expressed at very low levels in CAL-51 cells and were not identified (Figure S4A). Of the new target candidates, the protein with the greatest fold change and with a SAINT score of 1.0 was hexose-6-phosphate dehydrogenase (H6PD, G6PE, Figure 3G). H6PD, which resides in the endoplasmic reticulum (ER), catalyzes the conversion of glucose-6-phosphate to 6-phosphogluconate (Figure 5A), the rate-limiting step of the pentose phosphate pathway that generates precursors for nucleotide synthesis (Draper et al., 2003). Another critical function of H6PD is to maintain a high ratio of NADPH/$NADP^+$ within the ER.

Immunoblotting confirmed that H6PD was specifically enriched by the c-rucaparib affinity matrix and was fully competed with free rucaparib (Figure 5B). To determine the biochemical consequence of this interaction, we performed an *in vitro* H6PD activity assay, adapted from a literature assay that used hepatic cell lysates (Draper et al., 2003), with total lysate from both parental and H6PD-overexpressing HEK293 cells (Figure 5C). Lysates from parental HEK293 cells displayed no measurable H6PD activity. To eliminate possible interference from G6PD, which is responsible for carrying out the same reaction in the cytoplasm, the H6PD-specific substrate galactose-6-phosphate was employed. This assay confirmed inhibition of H6PD enzymatic activity by rucaparib with an IC_{50} of 18 μM, a rucaparib concentration that can be reached in mouse tumors (Murray et al., 2014), while no inhibition was evident with the other PARPi up to 100 μM.

Visual analysis of rucaparib's structure in comparison to the other PARPi suggests that the unique ability of rucaparib to inhibit H6PD may be attributed to one or more of its distinct structural features. These are most evident when rucaparib is overlaid with niraparib, which out of the three other PARPi, has the most similar structure (Figure 5D). Alignment of the benzamide pharmacophores highlights the constrained ring system formed by rucaparib's 7-membered lactam, the hydrogen bond donor provided by its unsubstituted indole nitrogen, and the electron-withdrawing fluorine at position 6 of the indole. The terminal aminomethyl group, though, is less likely to play a role for H6PD binding as this was modified by the tether attachment in c-rucaparib and this compound was still able to affinity capture H6PD.

Next, we assessed the potential contribution of H6PD inhibition to rucaparib's cellular activity. Stable overexpression of H6PD in CAL-51 cells increased the IC_{50} for inhibition of cell viability and rendered CAL-51 cells partially resistant to rucaparib, but not niraparib, suggesting a moderate contribution of H6PD inhibition towards rucaparib's overall cellular potency (Figure 5E). In addition, stable *H6PD* knockdown in CAL-51 cells increased the potency of olaparib and talazoparib, suggesting that targeting H6PD may cooperate with PARP1/2 inhibition (Figure 5F).

H6PD loss of function can cause apoptosis in cancer cells

To evaluate the relevance of H6PD as a cancer target, we assessed the cellular consequences of H6PD loss of function in CAL-51 cells. Transient knockdown of *H6PD* using either a specific shRNA hairpin (Figure 6A) or siRNA (Figure 6B), showed efficient silencing and increased cleavage of PARP1 and caspase-3 at 48 and more so at 72 h, indicating induction of apoptosis. Also, flow cytometry using Annexin V/DAPI showed a pronounced increase in early and late apoptotic cells after *H6PD* knockdown (Figure 6C). In addition, *H6PD* knockdown resulted in markedly reduced cell counts (Figure 6D). Consistent with this data, high concentrations of rucaparib, which can cause marked inhibition of H6PD, resulted in increased PARP1 and caspase-3 cleavage compared to the other PARPi (Figure 6E).

A cBioPortal analysis of publically available data, such as The Cancer Genome Atlas (TCGA) (Cerami et al., 2012), shows that whereas *H6PD* is not commonly altered in human tumors, gene amplification is detectable in several tumor types, most prominently in sarcoma, pancreatic and ovarian cancer, but also in lung adenocarcinoma, melanoma and breast cancer (Figure S4B). Therefore, we examined H6PD protein expression in a panel of breast cancer, adenocarcinoma non-small cell lung cancer (NSCLC), and melanoma cell lines, which are available in our lab. H6PD expression varied between cell lines and cancer types, but was present in all cell lines tested (Figure 7A). Whereas H6PD levels were relatively consistent across breast cancer cell lines, there were considerable differences across NSCLC cell lines, with the highest levels observed in H322 and H1648 cells. Interestingly, siRNA-mediated knockdown of *H6PD* in H322 cells showed, similar to CAL-51 cells, strong induction of apoptosis as indicated by PARP1 and caspase-3 cleavage (Figure 7B). However, despite efficient silencing, *H6PD* knockdown did not lead to apoptosis of MDA-MB-468 cells, indicating that not all cancer cells are sensitive to loss of H6PD (Figure 7C). Furthermore, at high rucaparib concentrations, which are expected to significantly inhibit H6PD, the viability of H322 cells is decreased more than with the same concentrations of the other PARPi. This is not the case for MDA-MB-468 cells (Figure 7D and 7E).

Discussion

In this study, we performed the first unbiased proteome-wide target profiling of the four clinical PARP inhibitors niraparib, olaparib, rucaparib and veliparib in CAL-51 breast cancer cells. Notably, although binding profiles may be somewhat different between cell lines, PARPi as a drug class display much higher target selectivity than other targeted therapeutic agents, in particular protein kinase inhibitors, which frequently have several dozen targets in a single cell type. Nonetheless, we observed several new target candidates for these PARPi beyond the PARP protein family; in total 17 new target candidates were identified. Of these candidates, two, DCK and H6PD, were functionally validated as direct targets of niraparib and rucaparib, respectively. Through this, we identified a novel anticancer target as well as a potential context-dependent therapeutic liability.

Our results regarding the target profiles within the PARP family show a high degree of consistency with previous reports (Wahlberg et al., 2012; Yang et al., 2013). Accordingly, we observed strong recovery of PARP1/2 as the primary targets of all four PARPi and, as

expected, also detected PARP4 and both tankyrases. Furthermore, we did not observe any PARP9-16 proteins interacting with olaparib, veliparib and rucaparib, which is consistent with the study by Wahlberg and colleagues (Wahlberg et al., 2012). One notable difference is PARP3, whose NAD^+ binding pocket is structurally different from PARP1/2 (Lehtio et al., 2009), and this difference likely prevents binding to our immobilized probe molecules. The potential for such a mismatch is a well-recognized inherent limitation of chemical proteomics (Rix and Superti-Furga, 2009). Conversely, our approach, which interrogates natural, full-length proteins at endogenous expression levels, successfully identified the known weaker interaction of olaparib with both tankyrase 1 and 2 (Menear et al., 2008; Narwal et al., 2012). These interactions were not captured by the otherwise comprehensive study using in vitro thermal shift assays with recombinantly expressed PARP catalytic domains (Wahlberg et al., 2012). However, both this approach and ours successfully identified the known interaction of rucaparib with tankyrase 1. Thus, PARP3 and the tankyrases illustrate the advantages, limitations and complementarity of the different technologies employed. No proteins from the NAD^+-binding sirtuin family were identified. This in agreement with a recent study where these PARPi were found to have no activity against sirtuins as the result of the planarity of their nicotinamide mimicking moieties (Ekblad and Schuler, 2016). This aspect may also contribute to the relatively high target selectivity of PARPi in general.

Another strength of chemical proteomics is the potential to identify robust protein complexes of engaged drug targets, as we and others have reported previously (Augustin et al., 2013; Bantscheff et al., 2007; Gridling et al., 2014; Sumi et al., 2015). IMPDH2 has not been previously identified as a PARP1/2 binding protein. However, a proteomics-based study recently identified both PARP1 and IMPDH2 as part of a base excision repair complex (Prasad et al., 2012). In addition, IMPDH2 has been found to be PARylated and to be a substrate of PARP1, 2, and 3 (Gagne et al., 2012; Gibson et al., 2016; Jungmichel et al., 2013), although the PARylation site on IMPDH2 is currently unknown. Further studies will be needed to determine the functional significance of the PARP/IMPDH2 interaction and whether it is influenced by PARP activity and PARylation.

The identification of a new (IMPDH2) and many known (e.g. LIG3, XRCC1/5/6) PARP1-binding proteins in our study highlights the ability of PARPi affinity matrices to interrogate PARP1- or PARP2-containing multiprotein complexes. For example, these compounds could be used to probe changes in PARP1 complex composition in different tumor types, after DNA damage or upon other cellular stress stimuli. Intriguingly, the high degree of selectivity for PARP1/2 over PARP3 of these probes could be useful for interrogating PARP1/2 complexes without “interference” by PARP3-binding proteins.

Previous studies have also reported the unexpected potential of some PARPi (e.g. rucaparib) to inhibit kinases, such as PIM1, DYRK1A or MLCK (Antolin and Mestres, 2014; McCrudden et al., 2015). We did not identify these particular targets in our experiments with CAL-51 cells, most likely due to their low expression in CAL-51 cells combined with relatively weak affinities. Of interest, though, we observed binding of two other kinases, CIT and DCK, with niraparib. Neither of these kinases was identified as a potential target of the

other three PARPi in our study. The inhibition of kinases by niraparib has not been reported, making this study the first to describe such a finding.

Inactivation of DCK through reduced expression or mutation causes resistance to the nucleoside analog anticancer drugs gemcitabine and cytarabine (Galmarini et al., 2001), illustrating that inhibition of DCK, while by itself known to be generally non-toxic, would be detrimental for therapeutic approaches with these types of cancer drugs. Thus, DCK can be considered a context-dependent anti-target of niraparib. As combinations of gemcitabine with olaparib or veliparib are being tested in clinical trials, caution should be exercised when applying similar drug combinations with niraparib. However, given the high concentrations needed to observe reduced cytarabine toxicity in our assay (20-40 μM), it is currently not clear whether niraparib would reach sufficiently high levels in tumor tissues to cause a significant degree of DCK inhibition.

Similar to DCK being only engaged by niraparib, we observed that H6PD is a unique target of rucaparib. We demonstrated that inhibition of H6PD plays a small but significant role for the overall cellular activity of rucaparib in CAL-51 cells and that *H6PD* knockdown can increase the potency of other PARPi. Although rucaparib plasma levels in patients are only 2.7 μM (Plummer et al., 2008), rucaparib concentrations in murine tumors were found to reach as high as ~20 μM (Murray et al., 2014), which is within the same range as the observed IC_{50} for H6PD inhibition. Drug concentrations in human tumor tissue are rarely available, but can be significantly higher (up to 40-fold) than the more accessible plasma levels, as was shown for the kinase inhibitor gefitinib (Haura et al., 2010). This suggests that H6PD could be measurably, albeit not completely, inhibited by rucaparib *in vivo*. This may be relevant because, even though the concentrations of PARPi needed to inhibit cellular PAR formation are in the low-to-midnanomolar range, others have demonstrated that the concentrations required to reduce cell viability are several orders of magnitude higher (Hopkins et al., 2015; Murai et al., 2014; Shen et al., 2013).

H6PD has been shown to be essential for maintaining a high NADPH/$NADP^+$ ratio in the ER, which drives 11β-hydroxysteroid dehydrogenase type 1 (11β-HSD1) reductase activity (Draper et al., 2003). 11β-HSD1 is a bi-directional enzyme that regulates pre-receptor glucocorticoid activation and is highly expressed in liver, adipose and skeletal muscle tissues. As a regulator of 11β-HSD1, H6PD plays a role in metabolic disorders such as obesity and type 2 diabetes, indicating the biological relevance of potential targeting by rucaparib (Banhegyi et al., 2009). In mice, *H6pd* knockout results in normal morphology and gestation, but causes a skeletal myopathy phenotype (Lavery et al., 2008b). In humans, homozygous inactivating *H6PD* mutations can cause cortisone reductase deficiency, but patients are otherwise healthy and skeletal myopathy has not been reported in these cases (Lavery et al., 2008a).

To the best of our knowledge, our study represents the first that shows potential utility of H6PD as a cancer target. Our knockdown results demonstrate that loss of H6PD can induce apoptosis in cancer cell lines, suggesting that loss of H6PD activity could lead to tumor cell death. However, not all cell lines are sensitive to *H6PD* knockdown, which illustrates the need to better understand its biology in the context of cancer, but also confirms that loss of

function does not cause general cytotoxicity. While the occurrence of *H6PD* gene amplification in human cancers is intriguing, a much larger study would be required to observe a correlation between expression level and sensitivity to loss of function. H6PD constitutes the first enzyme in the pentose phosphate pathway, which is important for nucleotide and nucleic acid synthesis. Given that *H6PD* knockdown can increase the potency of PARPi, which inhibit DNA repair, there could be a functional link between these pathways. Alternatively, H6PD inhibition may bypass the previously-reported rescue of PAR-mediated inhibition of hexokinase 1 by PARP inhibitors (Andrabi et al., 2014) and thereby lead to disruption of redox homeostasis and sensitivity to oxidative stress. Thus, in addition to being of interest in metabolic disorders, H6PD itself may constitute a novel anticancer target, either as a stand-alone target or with simultaneous disruption of DNA damage repair. A more potent H6PD inhibitor could contribute significantly to the study of the biology of H6PD in cancer and metabolic disorders, and for the development of new therapeutics for these diseases. As rucaparib is significantly more potent and selective than the only other known H6PD inhibitor genistein (reported IC_{50} > 50 μM) (Tagawa et al., 2015), and structural differences with other PARPi can be harnessed, rucaparib could be a useful starting point for developing more potent and specific H6PD inhibitors.

Significance

Selectivity is a key aspect for targeted drugs and small molecule probes, which has direct implications for their biological and clinical utility. There are several potent PARPi that are in clinical development and used as molecular probes, but their global and differential target selectivity has not been determined. Here, we describe the first side-by-side and proteome-wide target profile characterization of four clinically relevant PARP1 inhibitors, olaparib, veliparib, rucaparib and niraparib. We observed that PARPi in general display much higher target selectivity than has been reported for most other small molecule inhibitors, particularly kinase inhibitors. For both olaparib and veliparib, a high level of specificity for PARP1/2 was observed. This could be utilized for selective enrichment and investigation of PARP1/2 multiprotein complexes in different cellular contexts. In addition to the canonical targets PARP1, PARP2 and their binding partners, we identified new target candidates for niraparib and rucaparib. Subsequent functional validation suggested that inhibition of DCK by niraparib could have, depending on tumor drug concentrations, antagonistic effects when combined with nucleoside analogs. H6PD, an enzyme with a well-established role in metabolic disorders, was found to be a novel rucaparib target. In addition, our data suggest that H6PD may be a new cancer target, whose inhibition can augment the anticancer effects of PARP1/2 targeting. Importantly, rucaparib could serve as a novel starting point for the development of more potent and selective probe molecules and therapeutics for H6PD, which would be of great value in the study of its role in both cancer and metabolic diseases.

Methods

Detailed versions of all methods are available in the Supporting Information.

Synthesis of c-PARPi

Detailed synthetic protocols and characterization data can be found in the Supporting Information. C-veliparib, c-rucaparib, and c-niraparib were prepared from the parent drug via N-alkylation with *N*-(tert-butoxycarbonyl)-3-bromopropylamine followed by acidic BOC deprotection to yield the final c-PARPi. C-olaparib was prepared following a route analogous to the published preparation of olaparib, with diversion to c-olaparib at a late stage.

In Vitro PARP1 Activity Assay

Inhibition of PARP1 was assessed using the Universal Chemiluminescent PARP Kit. Luminescence readings were normalized to controls and fit to a sigmoidal dose response curve using GraphPad Prism 6 to determine IC_{50} values.

Cell Viability Assays

Cells were seeded into 384-well plates. After 24 h compound was added and cells were incubated at 37 °C 5% CO_2 for 3-5 days prior to analysis with CellTiterGlo. Cell viability was normalized to vehicle-treated wells and fit to a sigmoidal dose response curve using GraphPad Prism 6. Percent rescue from cytarabine toxicity was calculated by normalizing wells using PARP inhibitor-only treated wells or DI-39-only treated wells as 100% rescue and cytarabine only-treated wells as 0% rescue.

Cell Lysate Preparation for Proteomics and Co-Immunoprecipitation

Cells were harvested, pelleted by centrifugation and lysed with an equal volume of lysis buffer as described previously (Rix et al., 2007). The lysis mixture was centrifuged twice at 21,000xg and 4 °C (10 min, 20 min) and the protein concentra tion of the supernatant was determined using a Bradford assay.

Chemical Proteomics

Experiments were performed essentially as described before (Rix et al., 2007). All c-PARPi affinity experiments were performed as independent biological triplicates; ampicillin affinity enrichments were done in duplicate. c-Veliparib, c-niraparib, c-rucaparib, c-olaparib, and ampicillin were immobilized on NHS-activated beads and blocked overnight. Lysate was pre-incubated with competition compound or DMSO for 30 min at 4 °C. Affinity pulldown experiments were performed by incubating lysates for 2 h at 4 °C with drug-modified beads. After washing beads with lysis buffer, bound proteins were eluted by heating in Laemmli buffer. A portion of each eluate was set aside for immunoblotting. SDS-PAGE, in-gel digestion with trypsin and LC-MS/MS analyses were performed as described previously (Remsing Rix et al., 2014). Data was searched against the SwissProt 2015 human protein database using the Mascot search engine. Results were visualized in Scaffold 4.3.4. Peptides were analyzed as Exclusive Unique Spectrum Count, except where otherwise specified, and proteins were scored based on specificity (competition), relative abundance and reproducibility across replicates as defined in Table S1.

SAINT Analysis of Chemical Proteomics Data

Using Scaffold, the total spectra count for all proteins in each sample was exported and bait/inter/prey input files were prepared. For one analysis type, the PARPi affinity purification were compared against the competition purifications with free PARPi and the ampicillin purifications as control samples. For the other type of analysis, one PARPi purification sample set was compared to the other 3 PARPi purification sets as control samples. These input files were processed using SAINTexpress (Teo et al., 2014), and the fold-change and SAINT scores were plotted on a bubble graph, with the bubble size proportional to the Normalized Spectral Abundance Factors (NSAF) (Zybailov et al., 2007). The CRAPome probability score, which was used to color the bubbles, was calculated by first searching for each protein in the CRAPome database and then dividing the number of experiments where the protein is detected by the total number of experiments in the CRAPome (Mellacheruvu et al., 2013). Thus, a low CRAPome probability score corresponds to fewer instances identified as a contaminant in the CRAPome, and vice versa for a high score. For proteins that are not contained in the CRAPome database, a probability score of 0 was assigned.

Immunoblotting

Total cell lysates for immunoblotting were prepared as described above or with RIPA buffer. Proteins were resolved in polyacrylamide gels and transferred to activated PVDF using the TransBlot Turbo system. Membranes were blocked and probed with primary and secondary antibodies according to standard techniques. Detailed information on antibodies can be found in the Supporting Information.

Co-Immunoprecipitation

Protein A/G beads were rotated overnight at 4 °C wi th PARP-1, PARP-2 or rabbit IgG antibody. Beads were washed 3x with lysis buffer before addition of cell lysate, containing DMSO or 20 μM PARPi when used, and rotated at 4 °C for 4 h. Be ads were washed 4x with lysis buffer and proteins were heat-denatured in presence of Laemmli buffer. Beads were pelleted by centrifugation and the supernatant was used for immunoblotting.

H6PD Activity Assay

HEK293 H6PD-OE and HEK293 pellets were lysed and lysate was quantified with Bradford assay. Reaction mix containing galactose-6-phosphate (Gal6P) was combined with increasing concentrations of PARPi or DMSO. As an additional control, reaction mix without substrate was combined with HEK293 H6PD-OE lysate. Lysate from HEK293 or HEK293 H6PD-OE was added to each well to start the reactions. The absorbance at 340 nM (NADPH) was measured for 90 min at 10 min intervals. The 60 min data, which was within the linear range, was used for analysis. Background absorbance was subtracted and the H6PD activity of the HEK293 H6PDOE lysates treated with PARPi was normalized to the DMSO control. A detailed description of each control used and activity calculations is provided in the Supporting Information. Graphs were created in GraphPad Prism 6 using sigmoidal dose response (variable slope).

Virus Constructs and Viral Particle Preparation

Human *H6PD* was cloned into entry vector pENTR1A and recombined into destination vector pLenti-CMV-puro using Gateway LR Clonase II Enzyme mix. The resulting construct pLenti-CMV-H6PD$_{\text{short 3'UTR}}$ contains 0.6 kb of the original 3'UTR. Lentiviral constructs containing non-mammalian non-targeting shRNA control, human shH6PD$_{4374}$ (recognizes site 4374 in the 3'UTR of NM_004285.3, Broad Institute Clone ID TRCN0000234333) or human shPARP1$_{-2727}$ (recognizes site 2727 in the coding sequence of NM_001618.3, Broad Institute Clone ID TRCN0000338406) in lentiviral vector TRC2 pLKO were obtained from Sigma.

Virus was prepared by transfection of the constructs together with 3rd generation packaging mix vectors into HEK293T, concentrated by ultra-centrifugation and titered using a qPCR Lenti-viral titering kit.

Transient and Stable Knockdown and Overexpression

For transient or stable gene knockdowns, CAL-51 cells were transduced with shNT or human shH6PD$_{4374}$ virus. For overexpression, HEK293 and CAL-51 were transduced with the pLenti-CMV-H6PD$_{\text{short 3'UTR}}$ virus. Virus and polybrene were removed after 24 h, at which time drug treatment was started or selection for stable lines was initiated with puromycin.

Human *H6PD* SMARTpool siRNA and non-targeting control siRNA were transfected into CAL-51, H322, or MDA-MB-468 cells using Lipofectamine RNAiMAX according to manufacturers' instructions for reverse transfection.

DCK Activity Assay

Cellular protein was isolated from CCRF-CEM cells and whole cell lysates were incubated with ^{3}H-labeled deoxycytidine in the presence of varying concentrations of rucaparib, olaparib or niraparib. Reactions were performed at 37 °C in the presence of UTP and thymidine. After 30 minutes, the reactions were stopped by adding ice-cold water. The phosphorylated products were selectively bound to Whatman Grade DE81 ion exchange cellulose chromatography paper. After washing, radioactivity was measured using a beta-counter.

Supplementary Material

Refer to Web version on PubMed Central for supplementary material.

Acknowledgments

This work was supported by the H. Lee Moffitt Cancer Center and Research Institute, Miles for Moffitt and the V Foundation. We furthermore wish to acknowledge the Moffitt Chemical Biology (Chemistry Unit) and Proteomics Core Facilities, which are supported by the National Cancer Institute (Award No. P30-CA076292) as a Cancer Center Support Grant. Proteomics is also supported by the Moffitt Foundation and the Bankhead-Coley Cancer Research program of the Florida Department of Health (09BE-04). CR and WK were supported by a National Cancer Institute Grant R01 CA187678. CR is amongst the inventors of intellectual property for unrelated small molecule DCK inhibitors which have been licensed by the University of California to Trethera Corporation in which CR holds equity.

References

Andrabi SA, Umanah GK, Chang C, Stevens DA, Karuppagounder SS, Gagne JP, Poirier GG, Dawson VL, Dawson TM. Poly(ADP-ribose) polymerase-dependent energy depletion occurs through inhibition of glycolysis. Proc Natl Acad Sci U S A. 2014; 111:10209–10214. [PubMed: 24987120]

Antolin AA, Mestres J. Linking off-target kinase pharmacology to the differential cellular effects observed among PARP inhibitors. Oncotarget. 2014; 5:3023–3028. [PubMed: 24632590]

Augustin A, Lamerz J, Meistermann H, Golling S, Scheiblich S, Hermann JC, Duchateau-Nguyen G, Tzouros M, Avila DW, Langen H, et al. Quantitative chemical proteomics profiling differentiates erlotinib from gefitinib in EGFR wild-type non-small cell lung carcinoma cell lines. Mol Cancer Ther. 2013; 12:520–529. [PubMed: 23371860]

Banhegyi G, Csala M, Benedetti A. Hexose-6-phosphate dehydrogenase: linking endocrinology and metabolism in the endoplasmic reticulum. J Mol Endocrinol. 2009; 42:283–289. [PubMed: 19060178]

Bantscheff M, Eberhard D, Abraham Y, Bastuck S, Boesche M, Hobson S, Mathieson T, Perrin J, Raida M, Rau C, et al. Quantitative chemical proteomics reveals mechanisms of action of clinical ABL kinase inhibitors. Nat Biotechnol. 2007; 25:1035–1044. [PubMed: 17721511]

Bryant HE, Schultz N, Thomas HD, Parker KM, Flower D, Lopez E, Kyle S, Meuth M, Curtin NJ, Helleday T. Specific killing of BRCA2-deficient tumours with inhibitors of poly(ADP-ribose) polymerase. Nature. 2005; 434:913–917. [PubMed: 15829966]

Byers LA, Wang J, Nilsson MB, Fujimoto J, Saintigny P, Yordy J, Giri U, Peyton M, Fan YH, Diao L, et al. Proteomic Profiling Identifies Dysregulated Pathways in Small Cell Lung Cancer and Novel Therapeutic Targets Including PARP1. Cancer Discov. 2012; 2:798–811. [PubMed: 22961666]

Cerami E, Gao J, Dogrusoz U, Gross BE, Sumer SO, Aksoy BA, Jacobsen A, Byrne CJ, Heuer ML, Larsson E, et al. The cBio cancer genomics portal: an open platform for exploring multidimensional cancer genomics data. Cancer Discov. 2012; 2:401–404. [PubMed: 22588877]

Chuang HC, Kapuriya N, Kulp SK, Chen CS, Shapiro CL. Differential anti-proliferative activities of poly(ADP-ribose) polymerase (PARP) inhibitors in triple-negative breast cancer cells. Breast Cancer Res Treat. 2012; 134:649–659. [PubMed: 22678161]

Davis MI, Hunt JP, Herrgard S, Ciceri P, Wodicka LM, Pallares G, Hocker M, Treiber DK, Zarrinkar PP. Comprehensive analysis of kinase inhibitor selectivity. Nat Biotechnol. 2011; 29:1046–1051. [PubMed: 22037378]

Draper N, Walker EA, Bujalska IJ, Tomlinson JW, Chalder SM, Arlt W, Lavery GG, Bedendo O, Ray DW, Laing I, et al. Mutations in the genes encoding 11beta-hydroxysteroid dehydrogenase type 1 and hexose-6-phosphate dehydrogenase interact to cause cortisone reductase deficiency. Nat Genet. 2003; 34:434–439. [PubMed: 12858176]

Ekblad T, Schuler H. Sirtuins are Unaffected by PARP Inhibitors Containing Planar Nicotinamide Bioisosteres. Chem Biol Drug Des. 2016; 87:478–482. [PubMed: 26518726]

Farmer H, McCabe N, Lord CJ, Tutt AN, Johnson DA, Richardson TB, Santarosa M, Dillon KJ, Hickson I, Knights C, et al. Targeting the DNA repair defect in BRCA mutant cells as a therapeutic strategy. Nature. 2005; 434:917–921. [PubMed: 15829967]

Gagne JP, Pic E, Isabelle M, Krietsch J, Ethier C, Paquet E, Kelly I, Boutin M, Moon KM, Foster LJ, et al. Quantitative proteomics profiling of the poly(ADP-ribose)-related response to genotoxic stress. Nucleic Acids Res. 2012; 40:7788–7805. [PubMed: 22669911]

Galmarini CM, Mackey JR, Dumontet C. Nucleoside analogues: mechanisms of drug resistance and reversal strategies. Leukemia. 2001; 15:875–890. [PubMed: 11417472]

Gibson BA, Zhang Y, Jiang H, Hussey KM, Shrimp JH, Lin H, Schwede F, Yu Y, Kraus WL. Chemical genetic discovery of PARP targets reveals a role for PARP-1 in transcription elongation. Science. 2016; 353:45–50. [PubMed: 27256882]

Gridling M, Ficarro SB, Breitwieser FP, Song L, Parapatics K, Colinge J, Haura EB, Marto JA, Superti-Furga G, Bennett KL, et al. Identification of kinase inhibitor targets in the lung cancer microenvironment by chemical and phosphoproteomics. Mol Cancer Ther. 2014; 13:2751–2762. [PubMed: 25189542]

Haura EB, Sommers E, Song L, Chiappori A, Becker A. A pilot study of preoperative gefitinib for early-stage lung cancer to assess intratumor drug concentration and pathways mediating primary resistance. J Thorac Oncol. 2010; 5:1806–1814. [PubMed: 20881637]

Hopkins TA, Shi Y, Rodriguez LE, Solomon LR, Donawho CK, DiGiammarino EL, Panchal SC, Wilsbacher JL, Gao W, Olson AM, et al. Mechanistic Dissection of PARP1 Trapping and the Impact on In Vivo Tolerability and Efficacy of PARP Inhibitors. Mol Cancer Res. 2015; 13:1465–1477. [PubMed: 26217019]

Jungmichel S, Rosenthal F, Altmeyer M, Lukas J, Hottiger MO, Nielsen ML. Proteome-wide identification of poly(ADP-Ribosyl)ation targets in different genotoxic stress responses. Mol Cell. 2013; 52:272–285. [PubMed: 24055347]

Kaelin WG Jr. The concept of synthetic lethality in the context of anticancer therapy. Nat Rev Cancer. 2005; 5:689–698. [PubMed: 16110319]

Klaeger S, Gohlke B, Perrin J, Gupta V, Heinzlmeir S, Helm D, Qiao H, Bergamini G, Handa H, Savitski MM, et al. Chemical Proteomics Reveals Ferrochelatase as a Common Off-target of Kinase Inhibitors. ACS Chem Biol. 2016; 11:1245–1254. [PubMed: 26863403]

Laing RE, Walter MA, Campbell DO, Herschman HR, Satyamurthy N, Phelps ME, Czernin J, Witte ON, Radu CG. Noninvasive prediction of tumor responses to gemcitabine using positron emission tomography. Proc Natl Acad Sci U S A. 2009; 106:2847–2852. [PubMed: 19196993]

Lavery GG, Walker EA, Tiganescu A, Ride JP, Shackleton CH, Tomlinson JW, Connell JM, Ray DW, Biason-Lauber A, Malunowicz EM, et al. Steroid biomarkers and genetic studies reveal inactivating mutations in hexose-6-phosphate dehydrogenase in patients with cortisone reductase deficiency. J Clin Endocrinol Metab. 2008a; 93:3827–3832. [PubMed: 18628520]

Lavery GG, Walker EA, Turan N, Rogoff D, Ryder JW, Shelton JM, Richardson JA, Falciani F, White PC, Stewart PM, et al. Deletion of hexose-6-phosphate dehydrogenase activates the unfolded protein response pathway and induces skeletal myopathy. J Biol Chem. 2008b; 283:8453–8461. [PubMed: 18222920]

Lee JM, Ledermann JA, Kohn EC. PARP Inhibitors for BRCA1/2 mutation-associated and BRCA-like malignancies. Ann Oncol. 2014; 25:32–40. [PubMed: 24225019]

Lehtio L, Jemth AS, Collins R, Loseva O, Johansson A, Markova N, Hammarstrom M, Flores A, Holmberg-Schiavone L, Weigelt J, et al. Structural basis for inhibitor specificity in human poly(ADP-ribose) polymerase-3. J Med Chem. 2009; 52:3108–3111. [PubMed: 19354255]

McCrudden CM, O'Rourke MG, Cherry KE, Yuen HF, O'Rourke D, Babur M, Telfer BA, Thomas HD, Keane P, Nambirajan T, et al. Vasoactivity of rucaparib, a PARP-1 inhibitor, is a complex process that involves myosin light chain kinase, P2 receptors, and PARP itself. PloS one. 2015; 10:e0118187. [PubMed: 25689628]

Mellacheruvu D, Wright Z, Couzens AL, Lambert JP, St-Denis NA, Li T, Miteva YV, Hauri S, Sardiu ME, Low TY, et al. The CRAPome: a contaminant repository for affinity purification-mass spectrometry data. Nat Methods. 2013; 10:730–736. [PubMed: 23921808]

Mendes-Pereira AM, Martin SA, Brough R, McCarthy A, Taylor JR, Kim JS, Waldman T, Lord CJ, Ashworth A. Synthetic lethal targeting of PTEN mutant cells with PARP inhibitors. EMBO Mol Med. 2009; 1:315–322. [PubMed: 20049735]

Menear KA, Adcock C, Boulter R, Cockcroft XL, Copsey L, Cranston A, Dillon KJ, Drzewiecki J, Garman S, Gomez S, et al. 4-[3-(4-cyclopropanecarbonylpiperazine-1-carbonyl)-4-fluorobenzyl]-2H-phthalazin- 1-one: a novel bioavailable inhibitor of poly(ADP-ribose) polymerase-1. J Med Chem. 2008; 51:6581–6591. [PubMed: 18800822]

Murai J, Huang SY, Das BB, Renaud A, Zhang Y, Doroshow JH, Ji J, Takeda S, Pommier Y. Trapping of PARP1 and PARP2 by Clinical PARP Inhibitors. Cancer Res. 2012; 72:5588–5599. [PubMed: 23118055]

Murai J, Huang SY, Renaud A, Zhang Y, Ji J, Takeda S, Morris J, Teicher B, Doroshow JH, Pommier Y. Stereospecific PARP trapping by BMN 673 and comparison with olaparib and rucaparib. Mol Cancer Ther. 2014; 13:433–443. [PubMed: 24356813]

Murray J, Thomas H, Berry P, Kyle S, Patterson M, Jones C, Los G, Hostomsky Z, Plummer ER, Boddy AV, et al. Tumour cell retention of rucaparib, sustained PARP inhibition and efficacy of weekly as well as daily schedules. Br J Cancer. 2014; 110:1977–1984. [PubMed: 24556618]

Narwal M, Venkannagari H, Lehtio L. Structural basis of selective inhibition of human tankyrases. J Med Chem. 2012; 55:1360–1367. [PubMed: 22233320]

Nathanson DA, Armijo AL, Tom M, Li Z, Dimitrova E, Austin WR, Nomme J, Campbell DO, Ta L, Le TM, et al. Co-targeting of convergent nucleotide biosynthetic pathways for leukemia eradication. J Exp Med. 2014; 211:473–486. [PubMed: 24567448]

Overington JP, Al-Lazikani B, Hopkins AL. How many drug targets are there? Nat Rev Drug Discov. 2006; 5:993–996. [PubMed: 17139284]

Plummer R, Jones C, Middleton M, Wilson R, Evans J, Olsen A, Curtin N, Boddy A, McHugh P, Newell D, et al. Phase I study of the poly(ADP-ribose) polymerase inhibitor, AG014699, in combination with temozolomide in patients with advanced solid tumors. Clin Cancer Res. 2008; 14:7917–7923. [PubMed: 19047122]

Prasad R, Williams JG, Hou EW, Wilson SH. Pol beta associated complex and base excision repair factors in mouse fibroblasts. Nucleic Acids Res. 2012; 40:11571–11582. [PubMed: 23042675]

Remsing Rix LL, Kuenzi BM, Luo Y, Remily-Wood E, Kinose F, Wright G, Li J, Koomen JM, Haura EB, Lawrence HR, et al. GSK3 Alpha and Beta Are New Functionally Relevant Targets of Tivantinib in Lung Cancer Cells. ACS Chem Biol. 2014; 9:353–358. [PubMed: 24215125]

Rix U, Hantschel O, Durnberger G, Remsing Rix LL, Planyavsky M, Fernbach NV, Kaupe I, Bennett KL, Valent P, Colinge J, et al. Chemical proteomic profiles of the BCR-ABL inhibitors imatinib, nilotinib, and dasatinib reveal novel kinase and nonkinase targets. Blood. 2007; 110:4055–4063. [PubMed: 17720881]

Rix U, Superti-Furga G. Target profiling of small molecules by chemical proteomics. Nat Chem Biol. 2009; 5:616–624. [PubMed: 19690537]

Rouleau M, Patel A, Hendzel MJ, Kaufmann SH, Poirier GG. PARP inhibition: PARP1 and beyond. Nat Rev Cancer. 2010; 10:293–301. [PubMed: 20200537]

Savitski MM, Reinhard FB, Franken H, Werner T, Savitski MF, Eberhard D, Martinez Molina D, Jafari R, Dovega RB, Klaeger S, et al. Tracking cancer drugs in living cells by thermal profiling of the proteome. Science. 2014; 346:1255784. [PubMed: 25278616]

Scott CL, Swisher EM, Kaufmann SH. Poly (ADP-ribose) polymerase inhibitors: recent advances and future development. J Clin Oncol. 2015; 33:1397–1406. [PubMed: 25779564]

Shen Y, Rehman FL, Feng Y, Boshuizen J, Bajrami I, Elliott R, Wang B, Lord CJ, Post LE, Ashworth A. BMN 673, a novel and highly potent PARP1/2 inhibitor for the treatment of human cancers with DNA repair deficiency. Clin Cancer Res. 2013; 19:5003–5015. [PubMed: 23881923]

Strom CE, Johansson F, Uhlen M, Szigyarto CA, Erixon K, Helleday T. Poly (ADP-ribose) polymerase (PARP) is not involved in base excision repair but PARP inhibition traps a single-strand intermediate. Nucleic Acids Res. 2011; 39:3166–3175. [PubMed: 21183466]

Sumi NJ, Kuenzi BM, Knezevic CE, Remsing Rix LL, Rix U. Chemoproteomics Reveals Novel Protein and Lipid Kinase Targets of Clinical CDK4/6 Inhibitors in Lung Cancer. ACS Chem Biol. 2015; 10:2680–2686. [PubMed: 26390342]

Tagawa N, Kubota S, Kobayashi Y, Kato I. Genistein inhibits glucocorticoid amplification in adipose tissue by suppression of 11beta-hydroxysteroid dehydrogenase type 1. Steroids. 2015; 93:77–86. [PubMed: 25447798]

Teo G, Liu G, Zhang J, Nesvizhskii AI, Gingras AC, Choi H. SAINTexpress: improvements and additional features in Significance Analysis of INTeractome software. J Proteomics. 2014; 100:37–43. [PubMed: 24513533]

Tulin A. Re-evaluating PARP1 inhibitor in cancer. Nat Biotechnol. 2011; 29:1078–1079. [PubMed: 22158356]

Wahlberg E, Karlberg T, Kouznetsova E, Markova N, Macchiarulo A, Thorsell AG, Pol E, Frostell A, Ekblad T, Oncu D, et al. Family-wide chemical profiling and structural analysis of PARP and tankyrase inhibitors. Nat Biotechnol. 2012; 30:283–288. [PubMed: 22343925]

Yang KS, Budin G, Tassa C, Kister O, Weissleder R. Bioorthogonal approach to identify unsuspected drug targets in live cells. Angew Chem Int Ed Engl. 2013; 52:10593–10597. [PubMed: 23960025]

Ziegler S, Pries V, Hedberg C, Waldmann H. Target identification for small bioactive molecules: finding the needle in the haystack. Angew Chem Int Ed Engl. 2013; 52:2744–2792. [PubMed: 23418026]

Zybailov BL, Florens L, Washburn MP. Quantitative shotgun proteomics using a protease with broad specificity and normalized spectral abundance factors. Mol Biosyst. 2007; 3:354–360. [PubMed: 17460794]

Highlights

- Clinical PARP inhibitors display differential proteome-wide target selectivity.
- PARP inhibitors as a class have high target selectivity.
- Hexose-6-phosphate dehydrogenase (H6PD) is a new cancer-relevant rucaparib target.
- Deoxycytidine kinase (DCK) is a new context-dependent anti-target of niraparib.

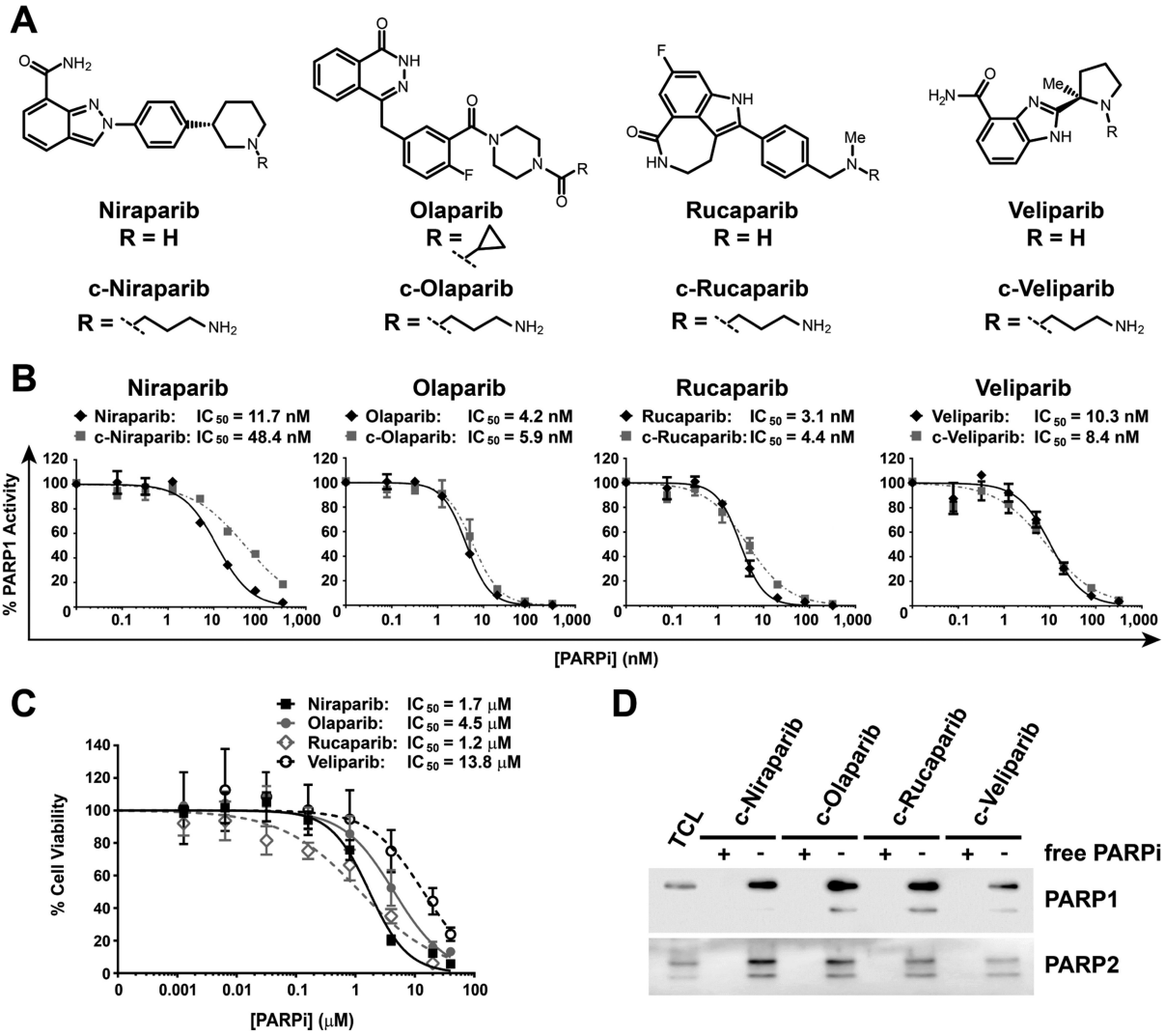

Figure 1. Synthesis and validation of linker-modified PARPi

(A) Structures of clinical PARP inhibitors and their modified coupleable derivatives (denoted by "c-" prefix) used for covalent attachment to NHS-sepharose beads. **(B)** *In vitro* inhibition of PARP1 activity by unmodified and coupleable versions of each PARPi, n = 3, s.e.m. **(C)** Inhibition of CAL-51 viability by PARPi, n = 5, s.d. **(D)** Immunoblots of eluates from PARPi-modified beads incubated with CAL-51 lysate ± 20 μM of the corresponding free PARPi (e.g. 20 μM niraparib added to c-niraparib matrix and lysate). Multiple bands arise from different isoforms of each protein. Blots are representative of three independent experiments. TCL: total CAL-51 cell lysate.

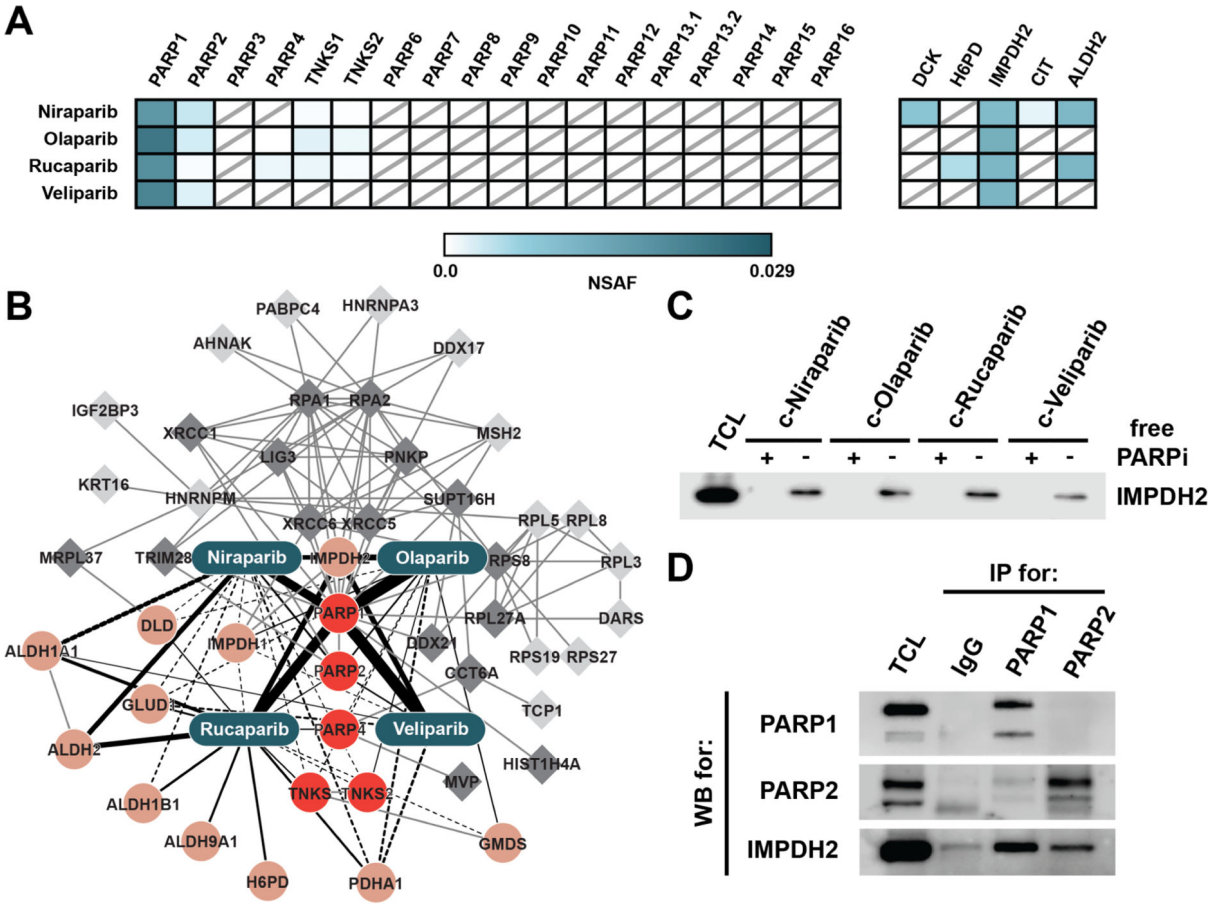

Figure 2. PARPi affinity matrices identify PARP1/2 protein complexes

(A) PARPs and other proteins identified as interacting with PARPi. Color indicates NSAF values for individual drug-protein interactions averaged across three replicates. **(B)** Drug-protein interaction network for olaparib, veliparib, rucaparib and niraparib in CAL-51 cells. Shown are all NAD(P)$^+$ binding proteins and their interactors that pass all 6 filtering criteria as specified in Table S3. PARP family proteins are depicted in red, NAD(P)$^+$-binding proteins in light red. Direct and indirect interaction partners of known or putative drug targets are shown in dark and light grey, respectively. Known and putative drug-protein interactions are represented by black edges, PPIs are shown in grey. PPIs between observed proteins were retrieved from public databases using the Cytoscape app BisoGenet. For drug-protein interactions, edge width indicates the respective NSAF value. Dashed edges indicate observed drug-protein interactions that do not pass all filtering criteria, but do so for interactions with other PARPi. IMPDH2 is depicted as interacting with all PARPi based on the proteomics data; its newly identified interaction with PARP1 is indicated by a solid grey edge. **(C)** Anti-IMPDH2 immunoblot of eluates from c-PARPi-modified beads incubated with CAL-51 lysate ± 20 μM corresponding free PARPi (e.g. 20 μM niraparib added to c-niraparib matrix and lysate). TCL: total CAL-51 cell lysate. **(D)** Immunoblots of PARP1, PARP2 and rabbit IgG immunoprecipitates from CAL-51 cell lysate. Blots are representative of three independent experiments.

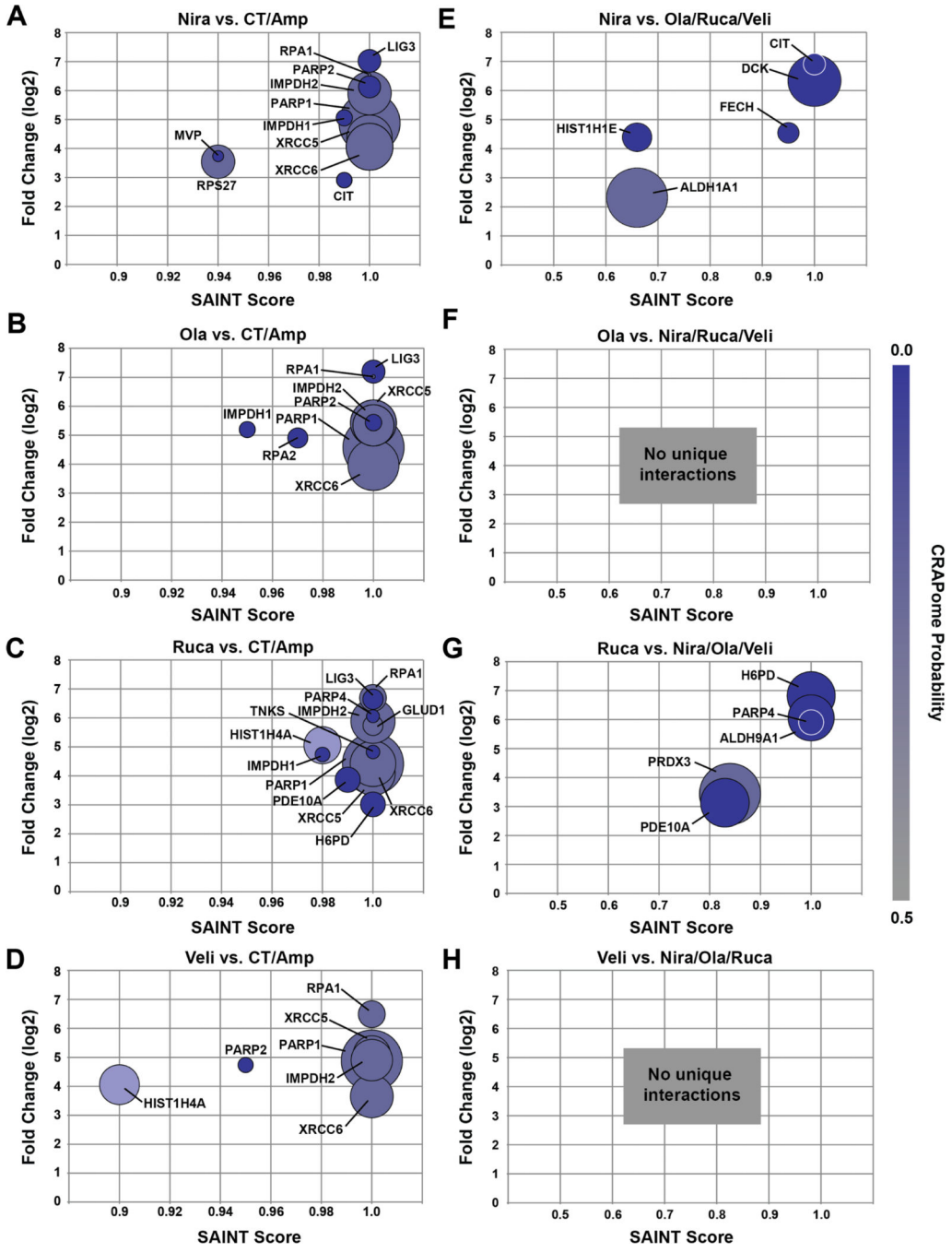

Figure 3. SAINTexpress analyses of all four PARPi

Fold change and SAINT score were calculated with SAINTexpress and all proteins with SAINT scores above 0.9 (**A-D**) or 0.5 (**E-H**) were plotted. Bubble size is proportional to the NSAF value and bubble color corresponds to CRAPome probability (scale 0-1, cutoff 0.5; low value: high probability for specific interaction; high value: high probability for non-specific interaction). No proteins yielded SAINT scores above 0.5 for the comparison of either olaparib or veliparib to the other three PARPi (**F** and **H**).

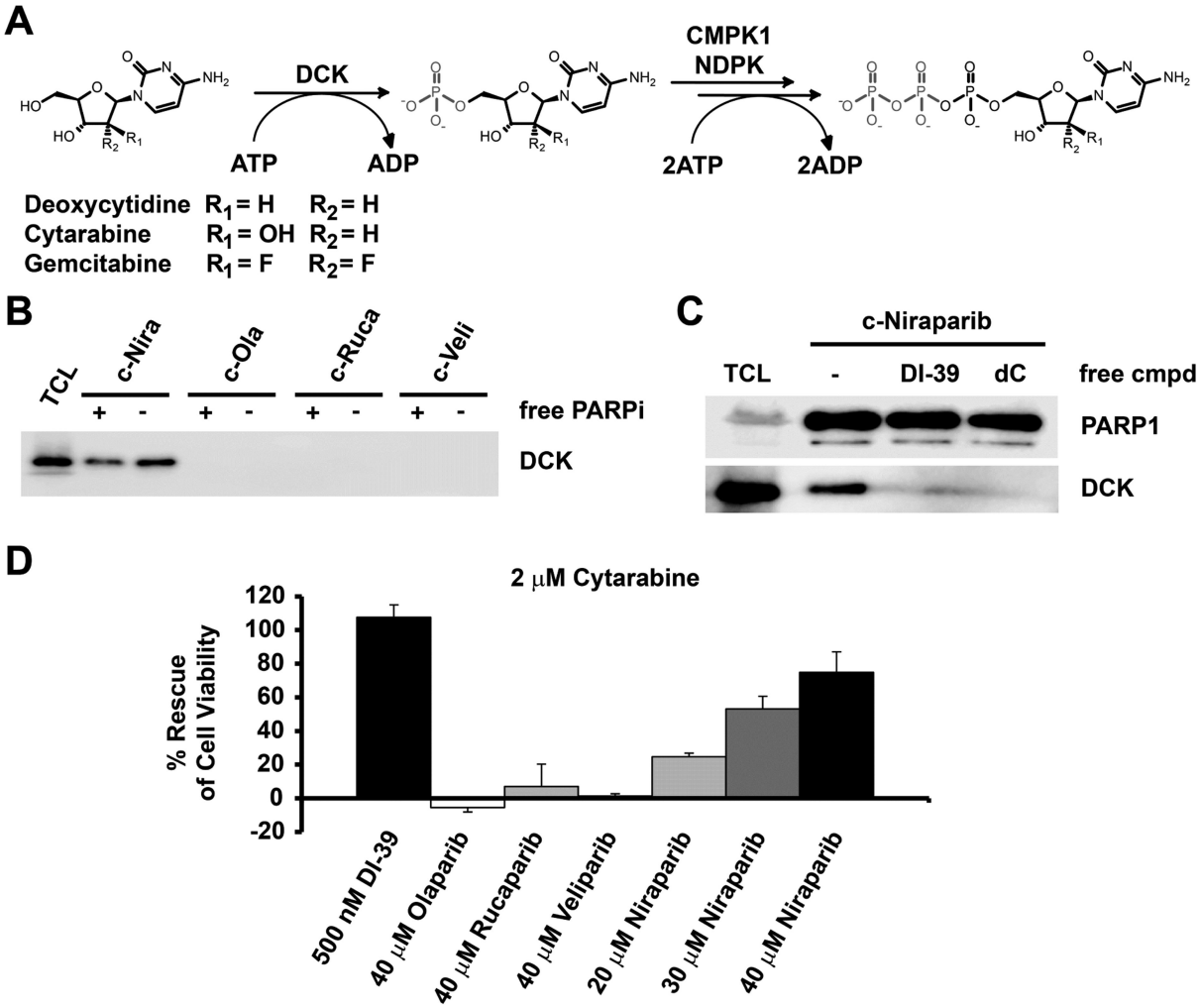

Figure 4. DCK is a new target of niraparib

(A) Schematic of DCK enzymatic activity and biosynthesis of nucleotide and nucleotide analog triphosphates. **(B)** Immunoblot of eluates from PARPi-modified beads incubated with CAL-51 lysate ± 20 μM of the corresponding free PARPi; blot is representative of two independent experiments. **(C)** Immunoblots of eluates from c-niraparib beads incubated with CAL-51 lysate ± 10 μM DCK inhibitor DI-39 or 1 mM DCK substrate deoxycytidine (dC). **(D)** Protection from cytarabine-induced toxicity. A549 cells were incubated for 3 days with 2 μM cytarabine ± the indicated concentrations of DCK inhibitor DI-39, niraparib, rucaparib, veliparib, or olaparib. Cell viability was measured by CellTiterGlo. Rescue was calculated by normalizing to the toxicity of cytarabine alone (0% rescue) and to cells incubated with PARPi or DI-39 only (100% rescue). n = 3, s.e.m.

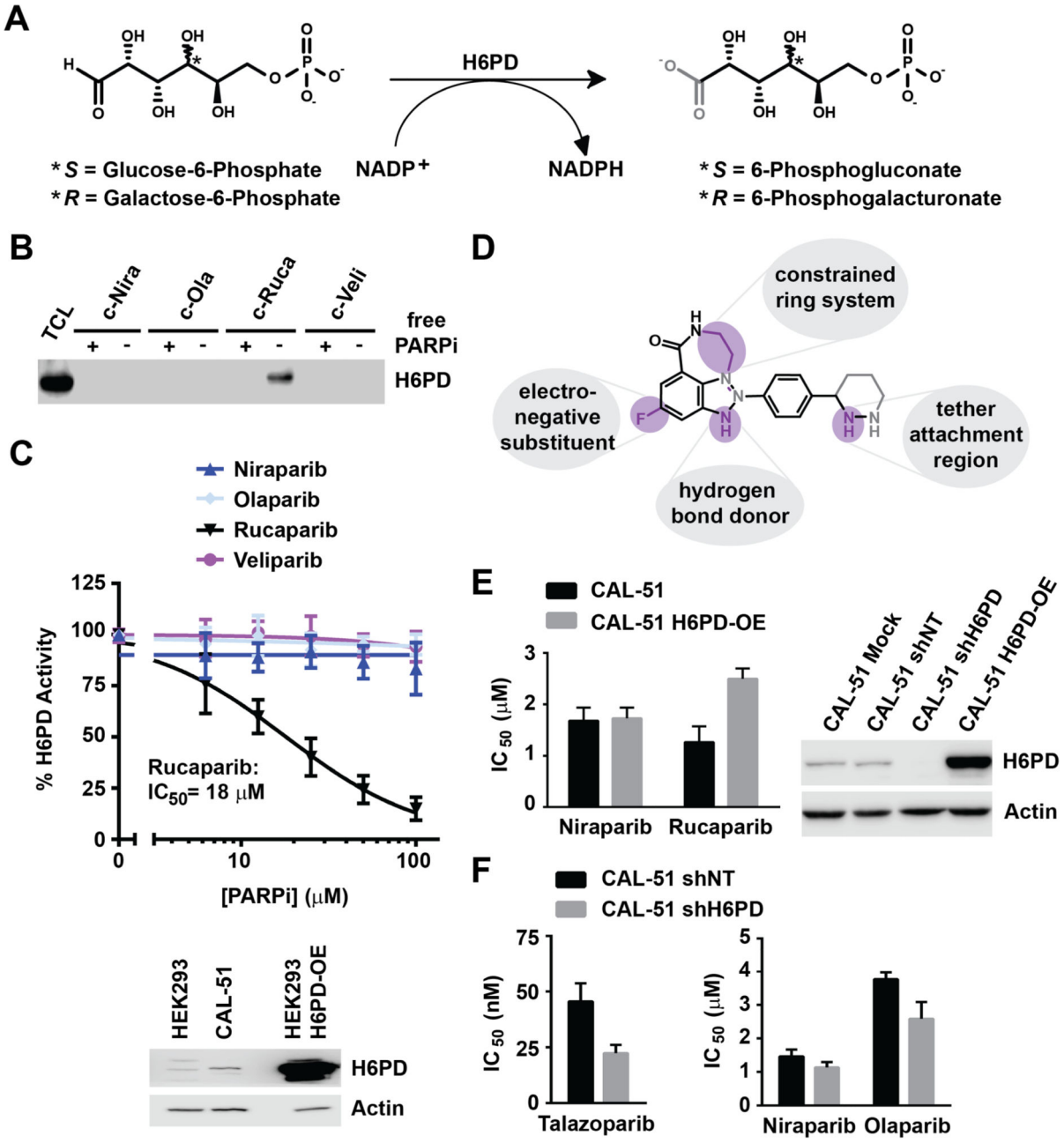

Figure 5. H6PD is a specific target of rucaparib

(A) Schematic of H6PD enzymatic activity for conversion of the natural substrate glucose-6-phosphate and the alternative H6PD-specific substrate galactose-6-phosphate. **(B)** Immunoblot of eluates from PARPi-modified beads incubated with CAL-51 lysate ± 20 μM of the corresponding free PARPi; blot is representative of two independent experiments. **(C)** H6PD activity in H6PD overexpressing (HEK293 H6PD-OE) cell lysate in the presence of increasing concentrations of PARP inhibitors. n = 5, s.d. Representative immunoblot for H6PD in both parental and overexpressing HEK293 cells is shown (bottom panel). **(D)** Overlay of rucaparib and niraparib structures. Shared features are shown in black, features unique to niraparib are shown in grey, and features unique to rucaparib are highlighted in

purple. **(E)** IC_{50} values for PARPi inhibition of cell viability were determined in parental CAL-51 cells and H6PD overexpressing (CAL-51 H6PD-OE) cells as measured by CellTiterGlo after 5 d, n = 5, s.e.m. **(F)** IC_{50} values for PARPi inhibition of cell viability were determined in CAL-51 shNT and CAL-51 shH6PD cell lines as measured by CellTiterGlo after 5 d, n = 5, s.e.m. Representative immunoblot for H6PD in CAL-51 mock, shNT, shH6PD and H6PD-OE cells is shown.

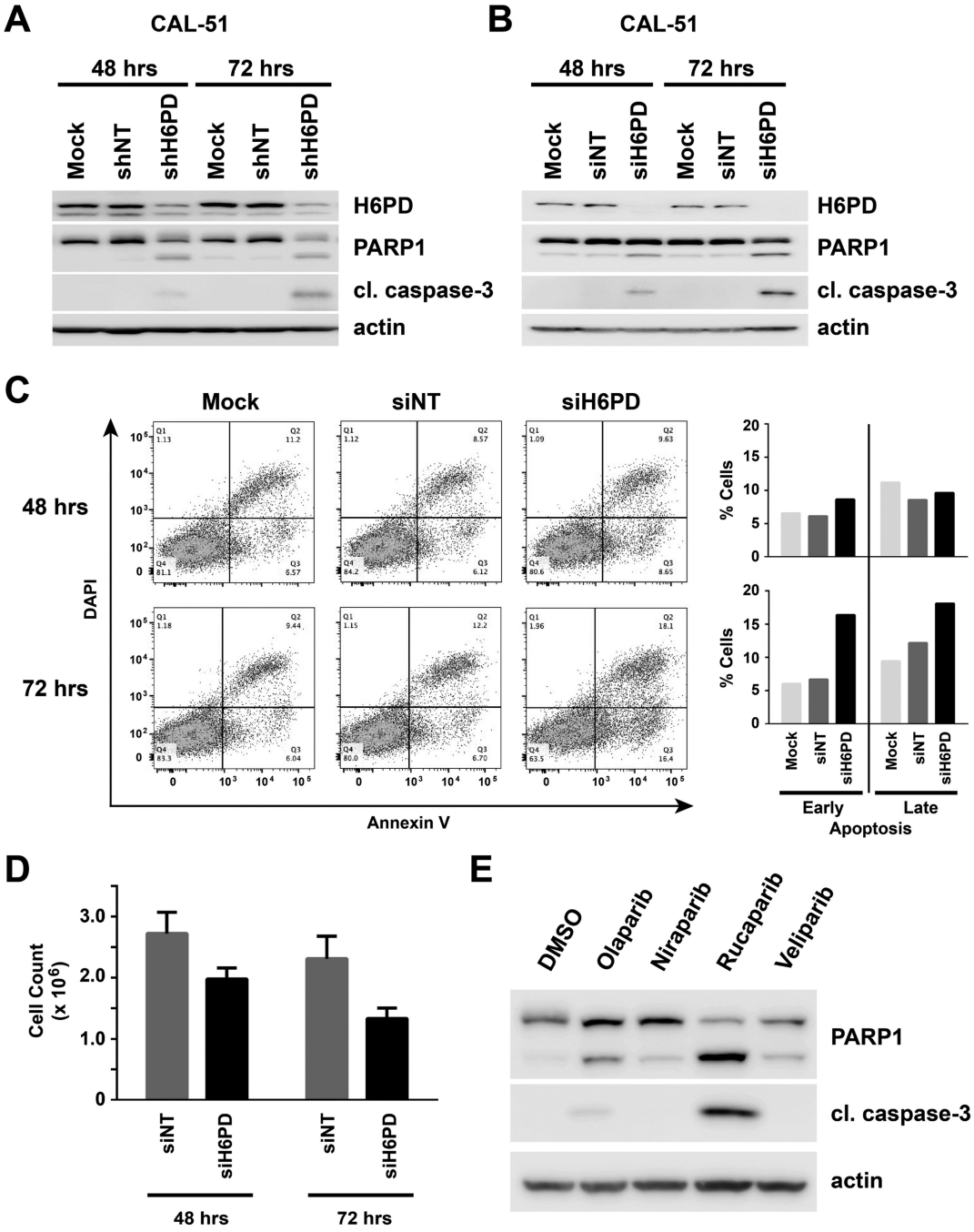

Figure 6. Loss of H6PD function causes apoptosis in CAL-51 cells

(A) Immunoblot analysis of transient shRNA-mediated *H6PD* knockdown in CAL-51 cells after 48 and 72 h. **(B)** Immunoblot analysis of siRNA-mediated *H6PD* knockdown in CAL-51 cells after 48 and 72 h. Blots are representative of three independent experiments (A, B). **(C)** Flow cytometry analysis of APC Annexin V/DAPI staining of CAL-51 cells 48 and 72 h after transfection with siNT or siH6PD. Right panel: quantification of cells in early apoptosis (Q3) and late apoptosis/necrosis (Q2). Data shown in density blots and their respective bar graphs correspond to one representative of three independent replicates. **(D)**

Number of viable CAL-51 cells after transfection with siNT or siH6PD at 48 and 72 h, n=4, s.e.m. **(E)** Immunoblot analysis of CAL-51 cells after 48 h treatment with 40 μM PARPi. Blots are representative of four independent experiments.

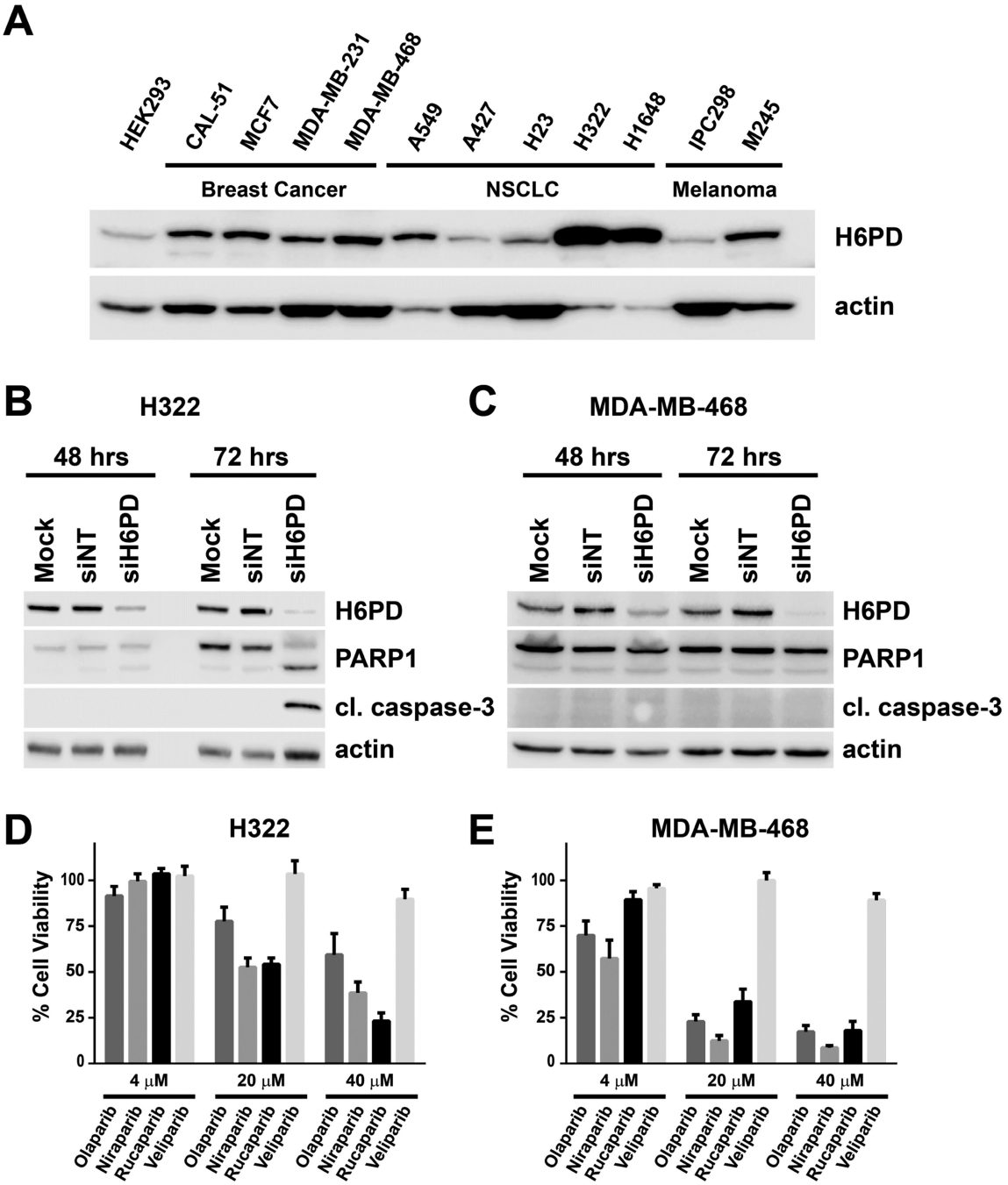

Figure 7. Loss of H6PD function causes apoptosis in some but not all cancer cells

(A) Immunoblot of relative H6PD levels in 11 cancer cell lines and HEK293 cells (included for comparison). **(B)** Immunoblot analysis of transient siRNA-mediated H6PD knockdown in H322 cells after 48 and 72 h. **(C)** Immunoblot analysis of transient siRNA-mediated H6PD knockdown in MDA-MB-468 cells after 48 and 72 h. Mock: transfection without siRNA; siNT: non-targeting siRNA; blots are representative of 2 independent experiments.

(D, E) Inhibition of H322 **(D)** and MDA-MB-468 **(E)** cell viability by PARPi as determined by CellTiterGlo after 5d, n = 3, s.e.m.